Molecular Therapy
Oncolytics
Original Article

Priming stroma with a vitamin D analog to optimize viroimmunotherapy for pancreatic cancer

Sang-In Kim,[1] Shyambabu Chaurasiya,[1] Venkatesh Sivanandam,[1] Seonah Kang,[1] Anthony K. Park,[2] Jianming Lu,[1] Annie Yang,[1] Zhifang Zhang,[1] Isabella A. Bagdasarian,[3] Yanghee Woo,[1,4] Joshua T. Morgan,[3] Zhirong Yin,[5] Yuman Fong,[1,4] and Susanne G. Warner[1,4]

[1]Department of Immuno-Oncology, Beckman Research Institute, City of Hope National Medical Center, 1500 E. Duarte Road, Duarte, CA 91010, USA; [2]Department of Hematologic Malignancies Translational Science, Beckman Research Institute, City of Hope National Medical Center, Duarte, CA 91010, USA; [3]Department of Bioengineering, University of California, Riverside, Riverside, CA 92521, USA; [4]Department of Surgery, Division of Surgical Oncology, City of Hope National Medical Center, 1500 E. Duarte Road, Duarte, CA 91010, USA; [5]Pathology Core, Department of Pathology, Beckman Research Institute, City of Hope National Medical Center, Duarte, CA 91010, USA

Pancreatic cancer resistance to immunotherapies is partly due to deficits in tumor-infiltrating immune cells and stromal density. Combination therapies that modify stroma and recruit immune cells are needed. Vitamin D analogs such as calcipotriol (Cal) decrease fibrosis in pancreas stroma, thus allowing increased chemotherapy delivery. OVs infect, replicate in, and kill cancer cells and recruit immune cells to immunodeficient microenvironments. We investigated whether stromal modification with Cal would enhance oncolytic viroimmunotherapy using recombinant orthopoxvirus, CF33. We assessed effect of Cal on CF33 replication using pancreas ductal adenocarcinoma (PDAC) cell lines and *in vivo* flank orthotopic models. Proliferation assays showed that Cal did not alter viral replication. Less replication was seen in cell lines whose division was slowed by Cal, but this appeared proportional to cell proliferation. Three-dimensional *in vitro* models demonstrated decreased myofibroblast integrity after Cal treatment. Cal increased vascular lumen size and immune cell infiltration in subcutaneous models of PDAC and increased viral delivery and replication. Cal plus serial OV dosing in the syngeneic Pan02 model caused more significant tumor abrogation than other treatments. Cal-treated tumors had less dense fibrosis, enhanced immune cell infiltration, and decreased T cell exhaustion. Calcipotriol is a possible adjunct for CF33-based oncolytic viroimmunotherapy against PDAC.

INTRODUCTION

Pancreatic ductal adenocarcinoma (PDAC) kills more than 90% of those afflicted.[1] PDAC progression can be slowed but not cured by the current cytotoxic chemotherapies.[2] In other words, chemotherapy alone is insufficient to produce a durable cure. It is crucial to identify and optimize radical immunogenic agents to galvanize and sustain antitumor immunity. In the immunosuppressive tumor microenvironment (TME) of PDAC, this requires a combination of stromal reprogramming and immune cell recruitment to give immunotherapy a fighting chance.[3–5]

Novel treatment paradigms are needed to promote both tumor destruction and antitumor immune responses. Oncolytic viruses (OVs) are strongly cytotoxic and immunogenic, which can directly kill tumor cells and modulate the TME to recruit and activate immune cells.[5–7] OV infection thereby renders the otherwise "cold" immunosuppressive TME of PDAC "hot" with inflammatory signals that recruit and activate immune cells.[3,5] This is especially true of double-stranded DNA viruses such as orthopoxviruses that induce immunogenic cell death.[6] We have engineered a recombinant orthopoxvirus platform (CF33) that overcomes many previously encountered barriers to successful viroimmunotherapy, such as potency and immunogenicity; this platform has been modified for real-time monitoring using reporter genes such as green fluorescent protein (GFP), firefly luciferase (Fluc), and human sodium iodide symporter (hNIS), as previously described.[8–13]

While viroimmunotherapy is clinically effective against immunogenic malignancies with abundant tumor-infiltrating lymphocytes, such as melanoma,[14] it is less effective against immunosuppressive PDAC.[15,16] More specifically, PDAC stroma is densely fibrotic, with few effector immune cells and abundant tumor-associated macrophages promoting and protecting tumor growth. In this context, stromal modulation may be beneficial both for enhanced delivery and immunogenicity. Because resistance to treatment is partly due to an immunosuppressive TME of PDAC, stromal modulation may permit targeted therapies to reach and destroy tumor cells more quickly.[17,18] By also allowing for more rapid conveyance of damage-associated signaling and resultant immune cells infiltration in the tumor, stromal reprogramming may facilitate antitumor immune activation.[18]

Received 8 October 2021; accepted 19 February 2022;
https://doi.org/10.1016/j.omto.2022.02.022.

Correspondence: Susanne G. Warner, Department of Immuno-Oncology, Beckman Research Institute, City of Hope National Medical Center, 1500 E. Duarte Road, Duarte, CA, 91010, USA.
E-mail: warner.susanne@mayo.edu

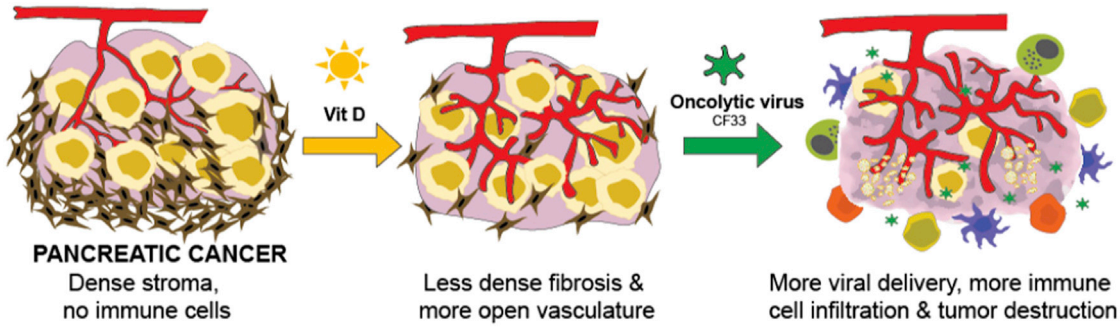

Figure 1. Hypothesis

Vitamin D analogs can decrease the density of pancreatic cancer stroma, allowing for enhanced oncolytic virus delivery and resultant immune cell infiltration and tumor destruction.

Vitamin D (VitD) analogs modulate PDAC stroma by activating VitD receptor (VDR), attenuating pro-tumor signaling, increasing tumor vasculature, and decreasing fibrosis.[17,18] In preclinical models, the VitD analog calcipotriol (Cal) enhances the delivery and efficacy of chemotherapy;[17] this concept is currently being studied in clinical trials (e.g., NCT03520790). However, even enhanced chemotherapy is likely to remain palliative without adjunctive immunogenic treatments to promote antitumor immunity. Because VitD analogs are historically considered to be antiviral due to their modulation of antiviral interferon responses, among other mechanisms, they have not been studied as oncolytic viral adjuncts.[19–21] However, we have shown that viruses derived from CF33 replicate unhindered in the presence of Cal.[22,23] Given that treatment with Cal activates VDR in PDAC stroma and enhances the delivery of chemotherapy,[17] we asked whether this same stromal reprogramming could enhance OV delivery and immunogenicity (Figure 1). Here, we used the CF33 platform to address the hypothesis that Cal primes PDAC stroma to enhance OV delivery, tumor destruction, and immune cell recruitment and activation against pancreatic cancer. Using syngeneic and human xenograft models of PDAC in mice, we observed that Cal pretreatment decreased stromal fibrosis and enhanced OV delivery.

RESULTS

Cal does not inhibit CF33-hNIS replication

To evaluate whether Cal exerted an antiviral effect on CF33 platform replication, we used immortalized human pancreatic cancer cells with varied baseline VDR expression (Figure 2A): BxPC-3 is VD responsive (VDR high), while Panc-1 is non-responsive (VDR low).[24] We tested our chimeric orthopoxvirus encoding the hNIS at the *J2R* locus (CF33-hNIS) at varied multiplicities of infection (MOIs) and found no direct inhibition of viral replication and tumor cell killing as seen with the standard MTS cytotoxicity assay (data not shown). This was confirmed using viral growth assays (Figure 2B). As expected, we observed growth abrogation in Cal-treated BxPC-3 cells, and as a result, viral replication was commensurately diminished in the first 24 h. These findings were supported by the Ki67 proliferation assay, which showed growth abrogation in BxPC-3 cells treated with Cal but no effect on the proliferation of Panc-1 cells (Figure 2C). Therefore, the differences in viral replication between BxPC-3 and Panc-1 cells with and without Cal were attributed to the baseline VD-responsive nature of these cells. We further assessed these findings in a Panc-1 flank xenograft model and did not find any difference in tumor growth abrogation following viral infection with or without Cal treatment (Figure S1A). However, there was some evidence in this Panc-1 model demonstrating that the Cal + OV-treated group maintained higher viral titers despite similar tumor size compared to OV alone (Figure S1B).

Cal enhances virus dissemination and replication in a syngeneic PDAC model

Because part of our central hypothesis was that the immune and inflammatory effects of stromal reprogramming would affect response to the virus, we evaluated this question in an immune-competent setting using the Pan02-GFP model, despite the equivocal results in nude mice. Therefore, to assess whether Cal facilitated faster delivery and replication of CF33 platform viruses, we examined tumors infected with CF33-Fluc. Forty-eight hours after intravenous (i.v.) injection of CF33-Fluc in mice with or without Cal pretreatment, the mice underwent bioluminescent imaging and were then euthanized. The tumors were formalin fixed and stained with anti-vaccinia antibodies for immunofluorescence microscopy. Imaging demonstrated increased luminescence in Cal + OV-treated tumors (Figures 3A and 3B). Immunofluorescent staining of harvested tumors confirmed increased multifocal tumor penetrance of CF33-Luc, along with evidence of increased virus replication in Cal + OV-treated tumors (Figures 3C and 3D). Mice in the same treatment groups were followed long term after either single or serial OV dosing with or without Cal to assess whether this enhanced delivery affected survival. While a single dose of the virus did not significantly reduce tumor growth with or without Cal (Figure 3E), mice that received a second dose 49 days after the initial dose in the Cal + OV group showed tumor abrogation thereafter (Figure 3F).

Cal decreases the density of tumor stroma, enhancing baseline immune cell presence

To better understand the mechanisms of enhanced viral delivery, we performed a detailed histopathologic analysis of tumors treated with the virus with or without Cal pretreatment. We found significantly

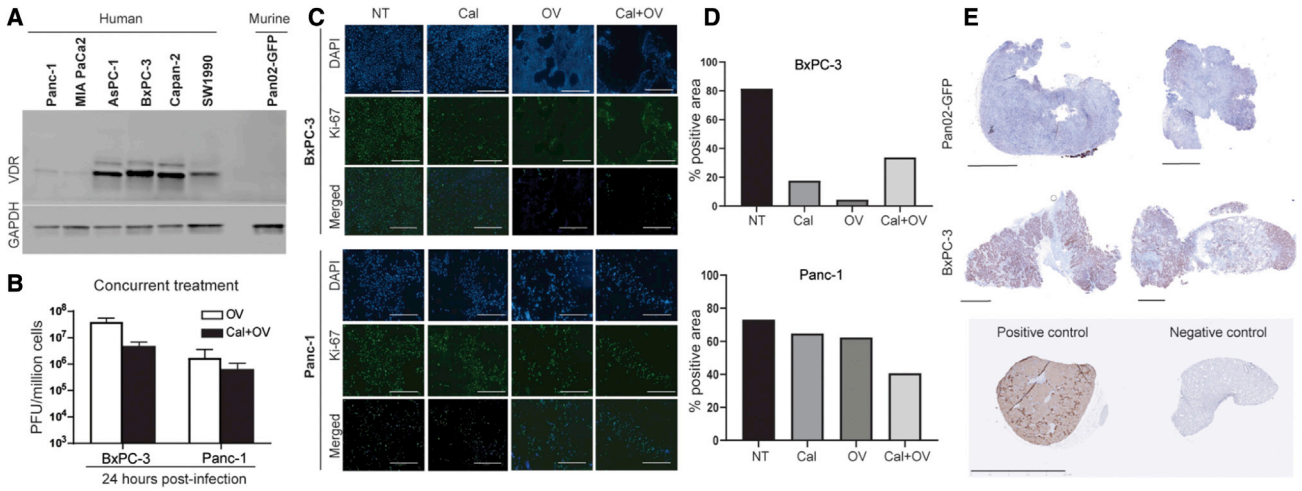

Figure 2. The vitamin D analog calcipotriol (Cal) does not directly affect replication of the oncolytic virus CF33

(A) Western blot showing baseline vitamin D receptor (VDR) expression in immortalized pancreatic cancer cell lines. (B) Viral titers at 24 h following infection of BxPC-3 or Panc-1 cells with CF33-hNIS alone (OV) or CF33-hNIS with concurrent Cal in ethanol preservative (Cal + OV). The error bars represent the standard deviation; stat = student's t-test was non-significant. (C) Ki67 staining demonstrates cell proliferation in BxPC-3 cells (upper panel) and Panc-1 cell proliferation (lower panel) with and without 100 nM Cal. Scale bar, 400 μm. (D) Ki67$^+$ area was quantified and compared among the different treatment groups. (E) IHC showing baseline VDR expression in tumor. Scale bar, 2.5 mm.

altered vascular and stromal morphology upon pathological evaluation (Figure 4A). This also held true for fibrosis. A representative set of slides shows that areas of strongest viral replication corresponded with those demonstrating lower density of activated (alpha-smooth muscle actin positive [α-SMA$^+$]) fibroblasts (Figure 4B). These changes were further evaluated and graded by an animal pathologist amalgamating cumulative findings from four representative slides per treatment group (Figure 4C). Interestingly, the quantity of staining for CD31$^+$ cells was similar between treatment groups despite morphologic changes (Figure 4D). However, α-SMA staining was significantly less prevalent in the OV-treated groups with and without the addition of Cal (Figure 4E). To understand whether Cal pretreatment was dose dependent, we evaluated histopathological changes of Panc-1 and BxPC-3 flank tumors after 5 or 10 days of pretreatment with Cal. We had hypothesized that we would see increased CD31 staining as an indicator of enhanced vasculature. Instead, we found similar rates of vascular density between groups, but that vascular morphology was distinct between groups with increases in vascular lumen size in Cal-treated groups, suggesting a decreased density of fibrosis. Representative slides of Panc-1 tumors are shown (Figure 4F), along with quantitation showing a pattern of increased vascular lumen area, which did not reach statistical significance (Figure 4G).

Three-dimensional (3D) modeling/signaling

Next, we wanted to better understand the interplay between fibroblasts, vascular epithelial cells, and cancer cells regarding viral infection. To achieve this, we performed experiments using a previously described 3D cell culture technique.[25] Briefly, a co-culture of fibroblasts, epithelial cells, and cancer cells was suspended in a 3-mg/mL collagen gel and cultured for 14 days with or without 500 nM Cal. Following pretreatment, the cells were incubated with OV for 24 h, fixed, and stained. With Cal pretreatment, we observed grossly visible fibroblast morphology changes (representative images shown in Figure S2). For the first time, we observed that OVs could infect and replicate in cells using this 3D organotypic culture. Subjectively, we observed increased virus delivery in the Cal-treated groups.

Tumor immune cell ratios after viral treatment demonstrate fewer regulatory T cells after Cal pretreatment

Next, we wanted to understand whether Cal pretreatment altered the known immune cell recruitment and activation induced by CF33-hNIS infection. C57Bl/6J mice bearing Pan02-GFP flank tumors were treated intraperitoneally (i.p.) for 3 days with either sham (PBS) or Cal (150 μg/kg) followed by i.v. injection with 3×10^7 plaque-forming units (pfu) of CF33-hNIS. To understand immune cell infiltration patterns, mice were euthanized 5 days following OV injection, and tumors were harvested and stained for CD3, CD8, and virus. Representative slides demonstrate increased CD3$^+$ and CD8$^+$ T cell infiltration in both OV alone and Cal + OV-treated groups compared to PBS-treated controls (Figure 5A). As previously seen, more viral replication was observed in additional areas of the Cal-pretreated tumor (Figure 5A). Whole-slide quantification confirmed significant increases in CD3$^+$ and CD8$^+$ T cells in both virus-treated groups, but it showed no significant immune cell quantitative differences in the Cal-pretreated group compared to the OV alone group (Figures 5B and 5C). To further understand the relationship of immune cell infiltration to Cal treatment, we compared Cal pretreatment against no treatment in the same Pan02-GFP model. We used multi-staining to more precisely assess immune cell status following Cal pretreatment. Intriguingly, significantly fewer FoxP3$^+$ regulatory T cells were observed in the Cal-pretreated group (Figure 5F). In addition,

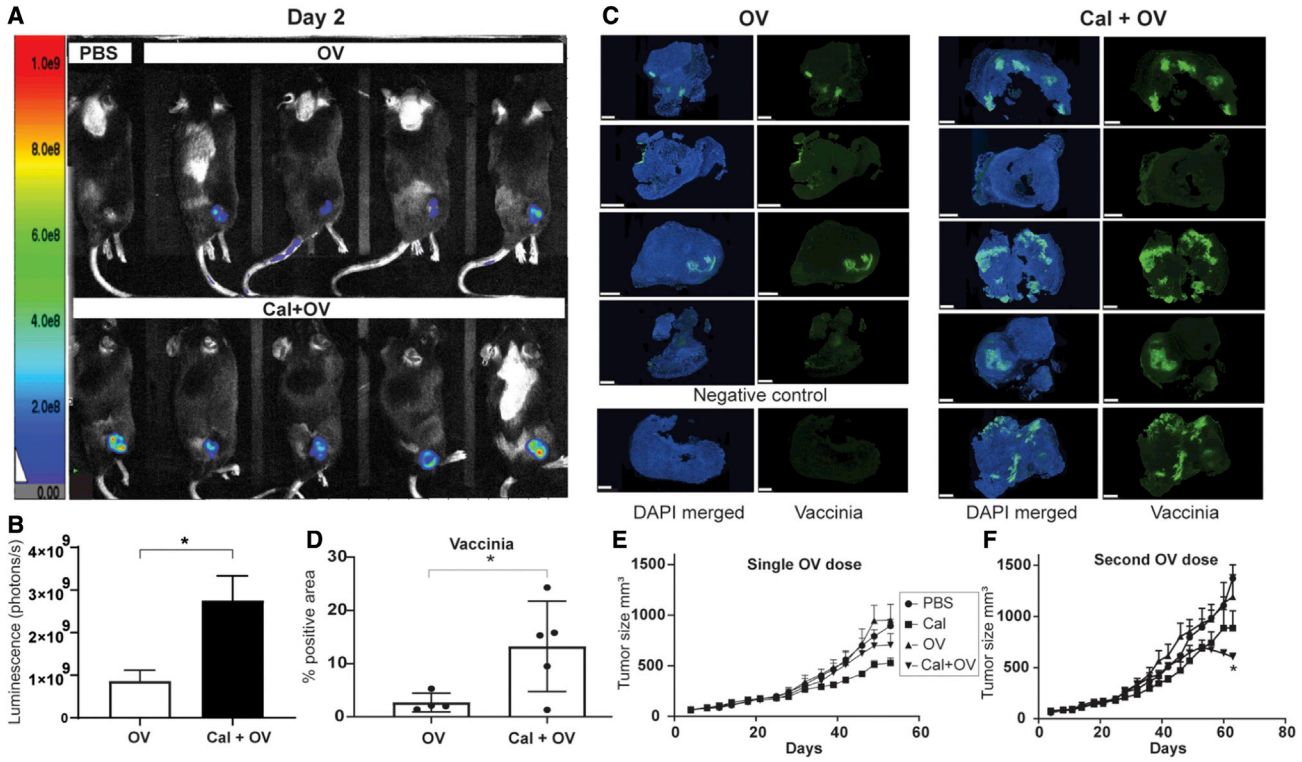

Figure 3. Cal enhances the delivery speed of the virus in the syngeneic Pan02-GFP model

(A and B) Qualitative (A) and (B) quantitative measurements of bioluminescent 48 h following mouse treatment with intravenous PBS, CF33-Fluc alone, or Cal pretreatment followed by CF33-Fluc. (C) Pathologic evaluation confirms increased viral staining (green) on immunofluorescence. Scale bar, 1 mm. (D) Virus-infected area (green) was quantified and compared between the 2 treatment groups. The error bars represent the standard error of the mean; stat, Welch's t test, *p < 0.05. (E and F) Tumor volume following a single dose of virus after at least 10 days of Cal pretreatment (E) and (F) tumor volume in mice treated with a second dose of virus following Cal pretreatment are shown. The error bars represent the standard error of the mean; stat, 1-way ANOVA, *p < 0.05.

observed but not consistently significant differences were seen in $CD4^+$ and $CD8^+$ staining (Figures 5D and 5E). Representative slides are shown in Figure 5G.

DISCUSSION

Here, we confirmed our hypothesis that pretreatment with the VitD analog Cal enhanced OV delivery, increased tumor destruction, and encouraged T cell infiltration into areas of increased vasculature and decreased fibrosis in a syngeneic PDAC model. Histopathologic findings demonstrate that pretreatment with Cal enhances CF33 delivery. These findings are also associated with dramatically altered morphology and function of vasculature and fibroblasts. Our results suggest that a serial dosing strategy could lead to more robust tumor growth abrogation. Paradoxically, despite the anti-inflammatory and known antiviral effects of VitD that can bolster antiviral immune responses,[21,26] CF33-induced immune cell infiltration appears undampened by VitD. Our investigations suggest that Cal pretreatment reduces regulatory T cells, possibly priming a microenvironment for viroimmunotherapy.

Our findings add to the literature by further confirming that PDAC "stromal softening" can enhance the speed of therapeutic delivery, as indicated by Sherman et al.[17,18] Because the administration of Cal has been shown to alter PDAC stroma by activating VDR and inducing cancer-associated fibroblast quiescence and decreasing the density of tumor fibrosis,[17] we hypothesized that Cal decreases the density of PDAC stroma, thereby enhancing the delivery of the virus. It follows that pretreatment with Cal would enhance virus delivery and drive oncolysis via easier access to tumor cells. Then, the same newly compliant neovascular pathways carrying the virus can also enhance immune cells infiltration in the tumor. Furthermore, antigen-presenting cells such as dendritic cells would have easy access to the pathogen-associated molecular pattern (PAMP) and damage-associated molecular pattern (DAMP) proteins resulting from the virus or the virus-mediated oncolysis, which would ultimately enhance antitumor immunity.[3] While our data did not delve into post-infection inflammatory signaling, as has been done by others examining immune escape and OVs,[27] we have laid the preliminary groundwork for further investigations in this space. Our data clearly show that VitD analog pretreatment results in faster and more robust tumor penetration of viruses. While many complex interactions contribute to this, we believe that this is most simply related to decreased tumor interstitial pressure caused by reduced fibrosis. This is supported by the fact that more virus staining was observed in the area of tumors that had a lower density of activated (α-SMA^+) fibroblasts. Our

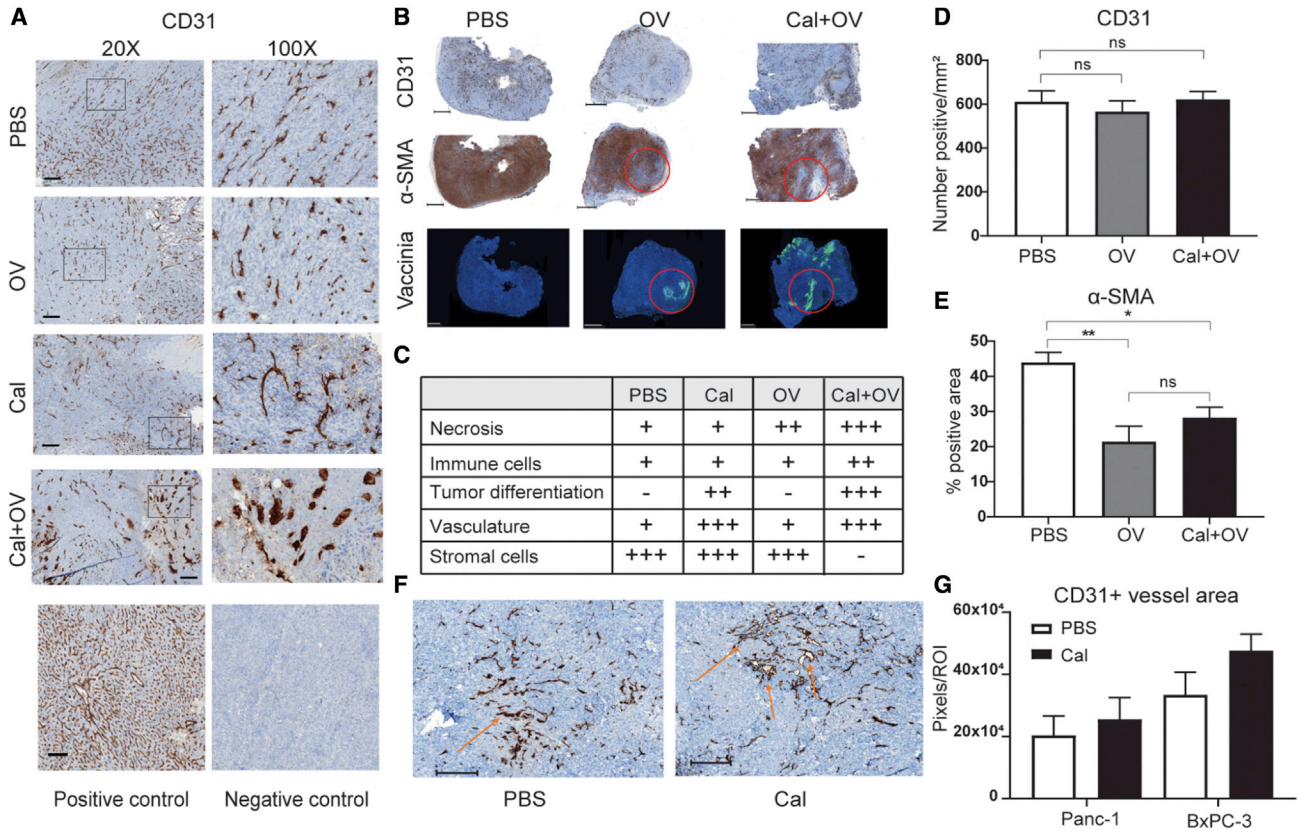

Figure 4. Cal enhances viral delivery via altered morphology of fibrosis and vasculature

(A) Mice bearing the syngeneic Pan02-GFP flank tumors treated with the virus or Cal alone or in combination demonstrate varied vascular morphology on immunohistochemical staining of vascular endothelium (CD31). Scale bar, 200 μm. (B) A whole-slide view from similar experiments using CF33-hNIS with or without Cal pretreatment shows an accumulation of the virus at areas of the tumor with less fibrosis as seen via α-SMA and vaccinia staining. Scale bar, 1 mm. (C) Qualitative assessment of the tumor is shown. (D and E) Quantification of the number of $CD31^+$ cells on whole-slide imaging. (E) α-SMA quantification is also shown. (F) In a nude mouse model, representative vascular morphologic changes between PBS and Cal-treated tumors are shown (scale bar, 400 μm), as are calculations for the vessel area (G) (n = 4/group). (D) and (E) Bars represent the standard error of the mean; stat, 1-way ANOVA; (G) Bars represent the standard error of the mean; stat, Welch's t test; *$p < 0.05$; **$p < 0.01$; ns, non-significant.

data further suggest that treatment with Cal results in increased vascular lumen size, which can be an indicator of decreased tumor pressure.[28] Our data are in agreement with the findings published in the seminal paper by Sherman et al., in which VitD analog was found to increase the vascular lumen size and resulted in better dissemination of gemcitabine within the PDAC vessel.[17]

It is difficult to contextualize these findings because very few investigations focus on the spatial orientation of virus replication in tumors. However, in a future clinical world in which we may be injecting 5 cm or larger tumors, it is critical to know precisely where in the tumor we need to target our next dose to maximize treatment efficacy.

We also show that VitD pretreatment in a syngeneic model decreases the number of regulatory T cells. Taken together, these data suggest that VitD-induced stromal remodeling may serve as a primer for OV infection in immunosuppressed TMEs. While others have suggested that Cal pretreatment decreases inflammatory signaling in a syngeneic PDAC TME, the complex interplay between Cal and tumor stroma is incompletely understood.[17] In a similar set of experiments using colon cancer models, we demonstrated decreased inflammatory signaling following Cal pretreatment.[23] Currently, we are attempting to elucidate the immune-inflammatory axis before and after virus infection in more clinically relevant models.

It should be noted that while Pan02-GFP is a syngeneic model, it has limitations for our purposes. Most notably, vaccinia does not robustly replicate in murine cells and has been shown to only weakly abrogate growth in a Pan02 model;[29] our *in vitro* cytotoxicity experiments have shown minimal cell killing in this model. That we were still able to achieve some measure of growth abrogation in this otherwise unresponsive model is remarkable. Another limitation for translating these findings to the clinic is the absence of the *Kras* mutation in the Pan02 model. Nevertheless, the immunogenicity and stromal changes seen with the addition of the VitD analog Cal are intriguing and have prompted further investigation in our laboratory.

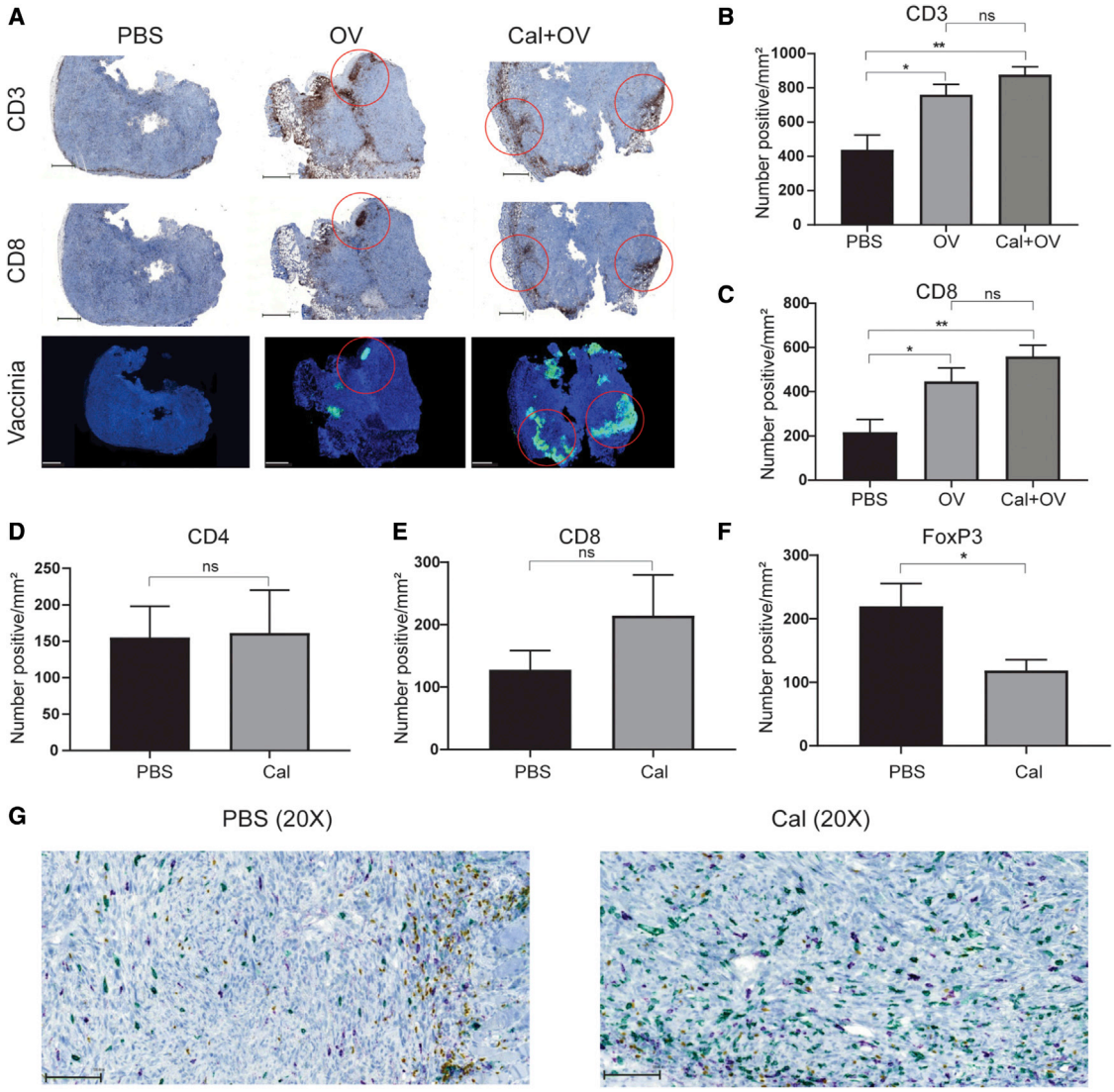

Figure 5. The oncolytic virus recruits T cells, and Cal decreases regulatory T cells in the tumor microenvironment

(A) Mice bearing syngeneic Pan02-GFP flank tumors treated with CF33-hNIS or Cal alone or in combination demonstrate an increased qualitative appearance of $CD3^+$ and $CD8^+$ in both virus-treated groups with T cells co-localizing to areas of viral replication. Scale bar, 1 mm. (B–F) Quantitative assessment of whole-slide staining demonstrated increased $CD3^+$ (B) and (C) $CD8^+$ cells in the virus-treated groups. The error bars represent the standard error of the mean; stat, 1-way ANOVA. Multi-staining quantification of (D) CD4, (E) $CD8^+$, and (F) $FoxP3^+$ cells is shown. (G) Representative slides are shown. Scale bar, 100 μm. The error bars represent the standard error of the mean; stat, Welch's test, *$p < 0.05$; **$p < 0.01$; ns, non-significant.

In summary, pretreatment with a vitamin D analog primes immunosuppressed or densely fibrotic TMEs of PDAC for efficient viroimmunotherapy. This may occur in part because stromal priming with Cal decreases regulatory T cells and fibrosis. Further studies are needed to understand how these findings interrelate with the immune-inflammatory axis in the context of other viruses and other PDAC models.

MATERIALS AND METHODS

The chimerization, cloning, competitive selection, and sequence of the CF33 backbone virus have been described previously.[9–12] Insertion of the hNIS expression cassette or Fluc under the control of the vaccinia H5 synthetic early (SE) promoter at the *J2R* locus has also been described.[10,11] CF33-GFP, also an H5 promoter at the *J2R* locus, has been used in some experiments.

Cell lines and mice

Panc-1, BxPC-3, MIA PaCa-2, Capan-2, AsPC-1, SW1990, and African green monkey kidney fibroblasts (CV-1) cell lines were purchased from the American Type Culture Collection (ATCC, Manassas, VA, USA). Pan02-GFP was purchased from GenTarget (San Diego, CA,

USA). All of the pancreatic cancer cell lines were cultured in Roswell Park Memorial Institute (RPMI) medium 1640 (Corning, Corning, NY, USA). CV-1 cells were maintained in Dulbecco's Modified Eagle's Medium (Corning). All of the cells were supplemented with 10% fetal bovine serum (FBS) and 1% antibiotic-antimycotic solution, both purchased from Corning. The cells were maintained in a humidified incubator at 37°C with 5% CO_2. All of the cell lines were tested for mycoplasma before the initiation of each experiment, and efforts were made not to perform experiments past 15 passages.

Six-week-old Hsd:Athymic Nude-Foxn1nu female mice (Envigo, Indianapolis, IN, USA) and 6- to 7-week-old C57Bl/6 female mice (Charles River, Wilmington, MA, USA) were used for the experiments. All of the mice were purchased and acclimatized for 7 days. The mice were maintained in a biosafety containment level 2 facility within our vivarium, where the environment was temperature and light controlled with 12-h light and 12-h dark cycles, and food and water were ingested *ad libitum*. All of the animal experiments were performed with the approval of the City of Hope Institutional Animal Care and Use Committee (IACUC, #15003).

Tumor models

For the athymic nude mouse models, flank tumors were generated by injecting 4–5 × 10^6 Panc-1 or BxPC-3 cells in a total of 100 μL PBS containing 50% Matrigel to create each tumor. When the average tumor volume approached approximately 150 mm^3, mice were divided into experimental groups and treated with 150 μg/kg of the VitD analog (Cal, Tocris, Bristol, UK) for 5 or 10 days by i.p. injection.

Flank tumors of Pan02-GFP were established using 1–5 × 10^5 cells in Matrigel. Treatment typically took place when tumors reached 50–200 mm^3 (approximately 5–10 days post-cell injection), following which mice were randomized into treatment groups such that the average tumor volume in each group was similar. Iterations of this experiment were performed with similar results. For all of the experiments, tumor measurements and mouse weight were monitored twice weekly using calipers to calculate tumor volume, V (mm^3) = (1/2) × A^2 × B, where A is the shortest measurement and B is the longest.

Western blotting

Protein was extracted from pancreatic cancer cells following cell washing and lysis. Next, 20 μg of each sample was fractionated on a Criterion Precast polyacrylamide gel (Bio-Rad, Hercules, CA, USA) and then transferred to a polyvinylidene fluoride (PVDF) membrane. The membrane was stained with anti-VitD receptor antibody (Cell Signaling Technologies, Danvers, MA) and horseradish peroxidase (HRP)-labeled goat anti-rabbit secondary antibody (Abcam, Cambridge, MA, USA) diluted 1:1,000 and 1:5,000, respectively, in iBind Flex solutions (Invitrogen, Waltham, MA, USA) overnight using the iBind Flex Western device (Thermo Fisher, Waltham, MA, USA) per the manufacturer's protocol. The membrane was then scanned using the Azure C600 scanner (Azure Biosystems, Dublin, CA, USA).

Viral growth assays

BxPC-3 and Panc-1 cells were seeded in 6-well plates (Corning) at 5 × 10^5 cells/well and incubated. The following day, the cells were counted and infected for 1 h at a MOI of 0.01 pfu per cell with CF33-hNIS in a total volume of 0.5 mL medium containing 2.5% FBS. The inoculum was aspirated, 2 mL fresh medium was added to each well, and the plates were returned to the incubator. In the concurrent treatment group, cells were treated with 100 nM Cal. After 24 h, cell lysates were collected by scraping, and virus titers were determined by the standard plaque assay, as described previously.[10]

Immunofluorescence

BxPC-3 and Panc-1 cells were incubated for 6 days with changing medium containing 100 nM Cal every 2 days to examine Ki67 expression. After the pretreatment of Cal, cells were treated with CF33-hNIS at an MOI of 3. Sixteen hours post-infection, cells were fixed and permeabilized with cold methanol for 15 min at −20°C and blocked for 30 min at room temperature in Tris-NaCl-blocking (TNB) buffer (0.1 M Tris-HCl, pH 7.5, 0.15 NaCl, and 0.5% blocking reagent, PerkinElmer, Waltham, MA, USA). After blocking, the cells were incubated with rabbit anti-Ki67 antibody [SP6] (Abcam) at a 1:250 dilution in TNB buffer and incubated overnight at 4°C. Cells were re-blocked in TNB buffer and stained with secondary goat anti-rabbit immunoglobulin G (IgG) H&L (heavy and light chains; Alexa Fluor 488) (Abcam) at a 1:500 dilution. Finally, 4′,6-diamidino-2-phenylindole (DAPI) was added and images were obtained using the EVOS FL Auto Imaging System (Thermo Fisher).

Luciferase imaging

Firefly luciferin solution was prepared per the manufacturer's instructions (PerkinElmer). Mice from all of the treatment groups, including control and CF33-Fluc-treated mice, received i.p. delivery of luciferin using the Lago X optical imaging system (Spectral Instruments Imaging, Tucson, AZ, USA) after 15 min of incubation.

Immunohistochemistry (IHC)

The tumors harvested at the time of sacrifice were fixed with 10% formalin. Subsequently, the tumors were paraffin embedded and 5-μm-thick sections were obtained. The slides were deparaffinized and stained on Ventana Discovery Ultra (Ventana Medical Systems, Roche Diagnostics, Indianapolis, IN, USA) IHC automated stainer, hematoxylin and eosin (H&E), VDR, CD3, CD8, CD31, α-SMA staining, multi-staining (CD4, CD8, and FoxP3), and pathological analysis were performed by the pathology core at the City of Hope National Medical Center. For vaccinia staining, the slides were deparaffinized, followed by heat-mediated antigen-retrieval per the manufacturer's protocol (IHC World, Ellicott City, MD, USA). Tumor sections were then permeabilized with methanol and blocked for 30 min with TNB buffer (PerkinElmer). Tumor sections were washed and incubated overnight in a humidified chamber at 4°C with a rabbit anti-vaccinia virus antibody (Abcam) 1:100 in TNB buffer. The next day, the tumor sections were stained with Alexa Fluor 488-conjugated goat anti-rabbit (Abcam) for 1 h at room temperature. Finally, the sections were counterstained with DAPI. Images were obtained using

the Ventana iScan HT (Roche, Basel, Switzerland) and the Nanozoomer 2.0-HT digital slide scanner (Hamamatsu Photonics, Hamamatsu City, Shizuoka Prefecture, Japan). Quantification of IHC staining was performed in conjunction with the light microscopy core at the City of Hope National Medical Center. The images were quantified with QuPath (Centre for Cancer Research & Cell Biology, Queen's University Belfast, UK) and Image Pro Premier (Media Cybernetics, Rockville, MD, USA) software. In concert with the molecular pathology core at the City of Hope National Medical Center, Visiopharm software (Visiopharm, Westminster, CO, USA) was used to quantify vascular lumen size in regions of interest.

Statistical analysis

Statistical analysis was performed using GraphPad Prism (version 7.01, GraphPad, La Jolla, CA, USA). Student's t test or one-way ANOVA were used to evaluate statistical significance. $p < 0.05$ was considered significant. Where present in the figures, the error bars indicate standard deviation (SD) or the standard error of the mean (SEM) as defined in the figure legends.

SUPPLEMENTAL INFORMATION

Supplemental information can be found online at https://doi.org/10.1016/j.omto.2022.02.022.

ACKNOWLEDGMENTS

Parts of this work were supported by the American Cancer Society Mentored Research Scholar Grant (MRSG-16-047-01-MPC). S.G.W. and S.C. are supported by the generosity of the Natalie and David Roberts Family (https://qupath.readthedocs.io/en/latest/docs/intro/citing.html). The authors would like to thank Michael Nelson of the City of Hope Light Microscopy Core for his guidance with IHC quantification. The authors are eternally grateful to Dr. Supriya Deshpande for her editorial assistance

AUTHOR CONTRIBUTIONS

Study concept & design, S.C., S.-I.K., V.S., Y.F., Y.W., A.K.P., J.T.M. Data collection, analysis, & interpretation, S.C., S.-I.K., V.S., I.A.B., J.T.M., J.L., S.K., Z.Y., Z.Z., A.Y., Y.F., and S.G.W. Manuscript preparation & critical revision, all of the authors. Final approval of manuscript, all of the authors.

DECLARATION OF INTERESTS

Y.F. receives royalties from Merck and from Imugene. The CF33 platform is licensed to Imugene by the City of Hope National Medical Center. The remaining authors are City of Hope employees but declare no competing interests.

REFERENCES

1. Rahib, L., Smith, B.D., Aizenberg, R., Rosenzweig, A.B., Fleshman, J.M., and Matrisian, L.M. (2014). Projecting cancer incidence and deaths to 2030: the unexpected burden of thyroid, liver, and pancreas cancers in the United States. Cancer Res. *74*, 2913–2921.

2. Gourgou-Bourgade, S., Bascoul-Mollevi, C., Desseigne, F., Ychou, M., Bouché, O., Guimbaud, R., Bécouarn, Y., Adenis, A., Raoul, J.-L., Boige, V., et al. (2013). Impact of FOLFIRINOX compared with gemcitabine on quality of life in patients with metastatic pancreatic cancer: results from the PRODIGE 4/ACCORD 11 Randomized Trial. J. Clin. Oncol. *31*, 23–29.

3. Gujar, S., Pol, J.G., and Kroemer, G. (2018). Heating it up: oncolytic viruses make tumors 'hot' and suitable for checkpoint blockade immunotherapies. OncoImmunology *7*, e1442169.

4. Carpenter, E., Nelson, S., Bednar, F., Cho, C., Nathan, H., Sahai, V., di Magliano, M.P., and Frankel, T.L. (2021). Immunotherapy for pancreatic ductal adenocarcinoma. J. Surg. Oncol. *123*, 751–759.

5. Russell, L., Peng, K.W., Russell, S.J., and Diaz, R.M. (2019). Oncolytic viruses: priming time for cancer immunotherapy. BioDrugs *33*, 485–501.

6. Heinrich, B., Klein, J., Delic, M., Goepfert, K., Engel, V., Geberzahn, L., Lusky, M., Erbs, P., Preville, X., and Moehler, M. (2017). Immunogenicity of oncolytic vaccinia viruses JX-GFP and TG6002 in a human melanoma *in vitro* model: studying immunogenic cell death, dendritic cell maturation and interaction with cytotoxic T lymphocytes. OncoTargets Ther. *10*, 2389–2401.

7. Chon, H.J., Lee, W.S., Yang, H., Kong, S.J., Lee, N.K., Moon, E.S., Choi, J., Han, E.C., Kim, J.H., Ahn, J.B., et al. (2019). Tumor microenvironment remodeling by intratumoral oncolytic vaccinia virus enhances the efficacy of immune-checkpoint blockade. Clin. Cancer Res. *25*, 1612–1623.

8. Chaurasiya, S., Yang, A., Kang, S., Lu, J., Kim, S.I., Park, A.K., Sivanandam, V., Zhang, Z., Woo, Y., Warner, S.G., et al. (2020). Oncolytic poxvirus CF33-hNIS-DeltaF14.5 favorably modulates tumor immune microenvironment and works synergistically with anti-PD-L1 antibody in a triple-negative breast cancer model. Oncoimmunology *9*, 1729300.

9. O'Leary, M.P., Choi, A.H., Kim, S.I., Chaurasiya, S., Lu, J., Park, A.K., Woo, Y., Warner, S.G., Fong, Y., and Chen, N.G. (2018). Novel oncolytic chimeric orthopoxvirus causes regression of pancreatic cancer xenografts and exhibits abscopal effect at a single low dose. J. Transl. Med. *16*, 110.

10. O'Leary, M.P., Warner, S.G., Kim, S.I., Chaurasiya, S., Lu, J., Choi, A.H., Park, A.K., Woo, Y., Fong, Y., and Chen, N.G. (2018). A novel oncolytic chimeric orthopoxvirus encoding luciferase enables real-time view of colorectal cancer cell infection. Mol. Ther. Oncolytics *9*, 13–21.

11. Warner, S.G. (2019). A novel chimeric poxvirus encoding hNIS is tumor-tropic, imageable, and synergistic with radioiodine to sustain colon cancer regression. Mol. Ther. Oncolytics *13*, 82–92.

12. Woo, Y., Zhang, Z., Yang, A., Chaurasiya, S., Park, A.K., Lu, J., Kim, S.I., Warner, S.G., Von Hoff, D., and Fong, Y. (2020). Novel chimeric immuno-oncolytic virus CF33-hNIS-antiPDL1 for the treatment of pancreatic cancer. J. Am. Coll. Surgeons *230*, 709–717.

13. Kim, S.I., Park, A.K., Chaurasiya, S., Kang, S., Lu, J., Yang, A., Sivanandam, V., Zhang, Z., Woo, Y., Priceman, S.J., et al. (2021). Recombinant orthopoxvirus primes colon cancer for checkpoint inhibitor and cross-primes T cells for antitumor and antiviral immunity. Mol. Cancer Ther. *20*, 173–182.

14. Andtbacka, R.H., Kaufman, H.L., Collichio, F., Amatruda, T., Senzer, N., Chesney, J., Delman, K.A., Spitler, L.E., Puzanov, I., Agarwala, S.S., et al. (2015). Talimogene laherparepvec improves durable response rate in patients with advanced melanoma. J. Clin. Oncol. : official J. Am. Soc. Clin. Oncol. *33*, 2780–2788.

15. Hecht, J.R., Bedford, R., Abbruzzese, J.L., Lahoti, S., Reid, T.R., Soetikno, R.M., Kirn, D.H., and Freeman, S.M. (2003). A phase I/II trial of intratumoral endoscopic ultrasound injection of ONYX-015 with intravenous gemcitabine in unresectable pancreatic carcinoma. Clin. Cancer Res. *9*, 555–561.

16. Noonan, A.M., Farren, M.R., Geyer, S.M., Huang, Y., Tahiri, S., Ahn, D., Mikhail, S., Ciombor, K.K., Pant, S., Aparo, S., et al. (2016). Randomized phase 2 trial of the oncolytic virus pelareorep (reolysin) in Upfront treatment of metastatic pancreatic adenocarcinoma. Mol. Ther. *24*, 1150–1158.

17. Sherman, M.H., Yu, R.T., Engle, D.D., Ding, N., Atkins, A.R., Tiriac, H., Collisson, E.A., Connor, F., Van Dyke, T., Kozlov, S., et al. (2014). Vitamin D receptor-mediated stromal reprogramming suppresses pancreatitis and enhances pancreatic cancer therapy. Cell *159*, 80–93.

18. Sherman, M.H., Yu, R.T., Tseng, T.W., Sousa, C.M., Liu, S., Truitt, M.L., He, N., Ding, N., Liddle, C., Atkins, A.R., et al. (2017). Stromal cues regulate the pancreatic cancer epigenome and metabolome. Proc. Natl. Acad. Sci. U S A *114*, 1129–1134.

19. Siddiqui, M., Manansala, J.S., Abdulrahman, H.A., Nasrallah, G.K., Smatti, M.K., Younes, N., Althani, A.A., and Yassine, H.M. (2020). Immune modulatory effects of vitamin D on viral infections. Nutrients *12*, 2879.

20. Fabri, M., Stenger, S., Shin, D.M., Yuk, J.M., Liu, P.T., Realegeno, S., Lee, H.M., Krutzik, S.R., Schenk, M., Sieling, P.A., et al. (2011). Vitamin D is required for IFN-gamma-mediated antimicrobial activity of human macrophages. Sci. translational Med. *3*, 104ra102.

21. Huang, J.F., Ko, Y.M., Huang, C.F., Yeh, M.L., Dai, C.Y., Hsieh, M.H., Huang, C.I., Yang, H.L., Wang, S.C., Lin, Z.Y., et al. (2017). 25-Hydroxy vitamin D suppresses hepatitis C virus replication and contributes to rapid virological response of treatment efficacy. Hepatol. Res. *47*, 1383–1389.

22. LaRocca, C.J., and Warner, S.G. (2018). A new role for vitamin D: the enhancement of oncolytic viral therapy in pancreatic cancer. Biomedicines *6*, 104.

23. Kim, S.I., Chaurasiya, S., Park, A.K., Kang, S., Lu, J., Woo, Y., Yin, H.H., Yin, Z., Fong, Y., and Warner, S.G. (2020). Vitamin D as a primer for oncolytic viral therapy in colon cancer models. Int. J. Mol. Sci. *21*, 7326.

24. Chiang, K.C., Yeh, C.N., Hsu, J.T., Yeh, T.S., Jan, Y.Y., Wu, C.T., Chen, H.Y., Jwo, S.C., Takano, M., Kittaka, A., et al. (2013). Evaluation of the potential therapeutic role of a new generation of vitamin D analog, MART-10, in human pancreatic cancer cells *in vitro* and *in vivo*. Cell Cycle (Georgetown, Tex) *12*, 1316–1325.

25. Morgan, J.T., Shirazi, J., Comber, E.M., Eschenburg, C., and Gleghorn, J.P. (2019). Fabrication of centimeter-scale and geometrically arbitrary vascular networks using *in vitro* self-assembly. Biomaterials *189*, 37–47.

26. Lange, C.M., Gouttenoire, J., Duong, F.H., Morikawa, K., Heim, M.H., and Moradpour, D. (2014). Vitamin D receptor and Jak-STAT signaling crosstalk results in calcitriol-mediated increase of hepatocellular response to IFN-alpha. J. Immunol. *192*, 6037–6044.

27. Evgin, L., Huff, A.L., Kottke, T., Thompson, J., Molan, A.M., Driscoll, C.B., Schuelke, M., Shim, K.G., Wongthida, P., Ilett, E.J., et al. (2019). Suboptimal T-cell therapy drives a tumor cell mutator phenotype that promotes escape from first-line treatment. Cancer Immunol. Res. *7*, 828–840.

28. Nagy, J.A., Chang, S.-H., Shih, S.-C., Dvorak, A.M., and Dvorak, H.F. (2010). Heterogeneity of the tumor vasculature. Semin. Thromb. Hemost. *36*, 321–331.

29. Hou, W., Sampath, P., Rojas, J.J., and Thorne, S.H. (2016). Oncolytic virus-mediated targeting of PGE2 in the tumor alters the immune status and sensitizes established and resistant tumors to immunotherapy. Cancer Cell *30*, 108–119.